CHIN. PHYS. LETT. Vol. 37, No. 5 (2020) 053201

Momentum Spectroscopy for Multiple Ionization of Cold Rubidium in the Elliptically Polarized Laser Field *

Junyang Yuan(袁俊阳)[1,2,3], Yixuan Ma(马祎璇)[1,2,3], Renyuan Li(李任远)[1,2], Huanyu Ma(马欢玉)[1,2,3], Yizhu Zhang(张逸竹)[1,4], Difa Ye(叶地发)[5], Zhenjie Shen(沈镇捷)[1], Tianmin Yan(阎天民)[1**], Xincheng Wang(王新成)[3**], Matthias Weidemüller[6,7,8], Yuhai Jiang(江玉海)[1,2,3,7**]

[1]*Shanghai Advanced Research Institute, Chinese Academy of Sciences, Shanghai 201210*
[2]*University of Chinese Academy of Sciences, Beijing 100049*
[3]*School of Physical Science and Technology, ShanghaiTech University, Shanghai 201210*
[4]*Center for Terahertz Waves and College of Precision Instrument and Optoelectronics Engineering, Key Laboratory of the Ministry of Education, Tianjin University, Tianjin 300072*
[5]*Laboratory of Computational Physics, Institute of Applied Physics and Computational Mathematics, Beijing 100088*
[6]*Hefei National Laboratory for Physical Sciences at the Microscale and Shanghai Branch, University of Science and Technology of China, Shanghai 201315*
[7]*CAS Center for Excellence and Synergetic Innovation Center in Quantum Information and Quantum Physics, University of Science and Technology of China, Shanghai 201315*
[8]*Physikalisches Institut, Universität Heidelberg, Im Neuenheimer Feld 226, 69120 Heidelberg, Germany*

(Received 10 February 2020)

Employing recently developed magneto-optical trap recoil ion momentum spectroscopy (MOTRIMS) combined with cold atoms, strong laser pulse, and ultrafast technologies, we study momentum distributions of the multiply ionized cold rubidium (Rb) induced by the elliptically polarized laser pulses (35 fs, 1.3×10^{15} W/cm^2). The complete vector momenta of Rb^{n+} ions up to charge state $n = 4$ are recorded with extremely high resolution (0.12 a.u. for Rb^+). Variations of characteristic multi-bands are displayed in momentum distributions because the ellipticity varies from the linear to circular polarization, are interpreted qualitatively with the classical over-barrier ionization model. Present momentum spectroscopy of cold heavy alkali atoms presents novel strong-field phenomena beyond the noble gases.

PACS: 32.80.Fb, 34.50.Fa, 32.80.Qk DOI: 10.1088/0256-307X/37/5/053201

The interaction of strong laser fields with atoms and molecules has attracted a large number of exciting phenomena in forefront strong-field physics, including above-threshold ionization (ATI),[1–4] sequential double ionization (SDI) and nonsequential double ionization (NSDI),[5–8] high-order harmonic generation,[9,10] and attosecond pulse creation.[11–14] To date, most theoretical and experimental studies are devoted to linearly polarized (LP) fields. Recently, a growing interest has been focused on the study of strong-field ionization induced by elliptically polarized (EP) fields,[15–18] as EP fields have the ability to uncover ionization information that is unreachable with LP fields. For example, by measuring the electron momentum from SDI, one can obtain information for the ionization fields and the release times of the emitted electrons,[19–21] which cannot be directly or easily obtained with LP fields. However, this can be straightforwardly obtained from the end-of-pulse recoil-ion momentum distributions (RIMDs) obtained under EP fields, even without the electron-ion coincidence detection.

Experimental techniques such as cold target recoil ion momentum spectroscopy (COLTRIMS)[22] and velocity map imaging (VMI)[23] have been used to measure RIMDs. In these techniques, an essential step is to cool the target to acquire RIMDs with high resolution. To our best knowledge, most experimental studies focus on rare or molecular gases, which can be cooled efficiently by supersonic gas jets. Alkali atoms have rarely been studied under the context of strong field processes, although the alkali atoms are featured for their low ionization energies and the easy manipulation of Rydberg states, which have been studied at room temperature.[24,25] After heating sublimation to gas phase, the thermal motion of targets will lead to poor momentum resolution for recoil-ions. In fact, preparing cold alkali atoms with magneto-optical-trap (MOT) technique is a routine for high momentum resolution. Combining the MOT technique with a COLTRIMS, we set up a MOTRIMS platform which is an integration of ultracold atom and momentum imaging,[26] to effectively study the ultrafast processes within alkali or alkaline-earth atoms that otherwise cannot be cooled by conventional supersonic gas jets. In atomic, molecular, and optical (AMO) physics, MOTRIMS is available in studying various aspects of the electron capture process: examples are inner-shell and outer-shell electron captures,[27,28] photoassociation in cold atoms,[29] ion-atom/molecule and photon atom/molecule collisions.[30] Beyond AMO physics, MOTRIMS is also used for precision measurements in nuclear physics.[31,32] To date, there is no report on MOTRIMS apparatus combined strong and ultrafast

*Supported by the National Natural Science Foundation of China (Grant Nos. 11827806, 11874368, 61675213, 11822401, and 11674034).
**Corresponding author. Email: jiangyh@sari.ac.cn; wangxch1@shanghaitech.edu.cn; yantm@sari.ac.cn
© 2020 Chinese Physical Society and IOP Publishing Ltd

laser fields that focus on the multiple ionization process. Thus, the combination of these three advanced techniques (i.e., COLTRIMS, MOT, and the femtosecond pulse) presents an acutely powerful experimental tool for the study of momentum spectroscopy for heavy alkali atoms in the strong-field physics, being novel investigations in the multi-dimensions beyond the noble gases.[33]

In this Letter, we study strong field multiple ionization of Rb targets in EP fields with our MOTRIMS setup. The neutral Rb atoms are ionized up to Rb^{4+} and the RIMDs are reconstructed with extremely high resolution (0.12 a.u. for Rb^{+}). The momentum distributions exhibit rich multi-band structures as the ellipticity varies from the LP to close-to circularly polarized (CP) fields. With the help of the classical over-barrier ionization model, we analyze experimental observations and identify underlying mechanisms.

The experimental setup is based on a double-chamber system, with a Rb atom source prepared in a glass cell and then delivered to the target region of the science chamber. In the glass cell, Rb atoms are pre-cooled within a typical two-dimensional magneto-optical trap (2D MOT) configuration, and then pushed by a laser beam into the target region, where it can be further cooled and trapped with a standard three-dimensional magneto-optical trap (3D MOT) configuration. Either the 3D MOT target, molasses or the 2D MOT target with various densities can be selected within the target region. Detailed information about the experimental setup and target preparation is presented in Ref. [26]. The density of the molasses target used in this experiment is approximately 10^8 atoms/cm^3, and the background vacuum in the science chamber is lower than 2×10^{-10} mbar. The intense femtosecond laser pulses ($\sim$ 35 fs, 800 nm) are generated from a mode-locked Ti:sapphire laser system with a repetition rate of 1 kHz. A combination of a $\lambda/2$ plate and an alpha-BBO Glan-Taylor laser polarizer is employed to adjust the incident laser intensity. The peak intensity I is calibrated by measuring the "donut"-shape RIMDs of doubly charged Rb^{2+} with CP fields below the over-barrier ionization.[34] The uncertainty of I is estimated to be 20%. A zero-order quarter-wave plate is positioned at the entrance of the science chamber to polarize the laser with ellipticity ε. The polarized laser beam is focused by a concave mirror of 75 mm focal length onto the cold Rb molasses target. Varying the ellipticity at a constant intensity 1.3×10^{15} W/cm^2, the Keldysh parameter γ changes from 0.42 to 0.82 for all involved charge states. After ionization, the ions are accelerated by a homogeneous electric field ($\sim$1 V/cm) along the time-of-flight (TOF) axis toward a time- and position-sensitive microchannel plate (MCP) detector. The channel plate detector followed by a multi-hit anode allows extracting the information, including the TOFs and the positions on the detector where the ions arrived, by which the full vector momenta of these ions can be reconstructed.

A typical TOF spectrum for different charge states of Rb^{n+} is shown in Fig. 1. The recoil ions are identified in a time-of-flight (TOF) mass spectrometer according to their mass-to-charge ratio. It should be noted that we have adjusted the data recording TDC (time to digital convertor) such that the ions with TOF larger than Rb^{2+} are not recorded because the extremely high ionization rate of Rb^{+} results in large data storage and very slow data processing. The full widths at half maximum (FWHMs) for the peaks of Rb^{2+}, Rb^{3+} and Rb^{4+} are about 286 ns, 319 ns, 330 ns, respectively, which are at least one order narrower than the H_2O^{+} peak. The FWHMs represent an convolution of experimental resolution and physical effects, thus the lower limit of resolving power $m/\Delta m$ can be estimated. Here, taking Rb^{+}, a resolving power $m/\Delta m$ of 3000 was obtained in the present experimental settings.[26]

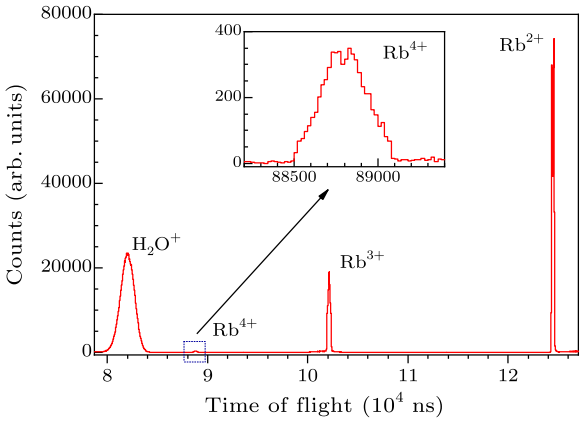

Fig. 1. The time-of-flight (TOF) spectrum of Rb ions. The peaks from right to left show the signals of Rb^{2+}, Rb^{3+}, Rb^{4+} and H_2O^{+} ions in intense close-to CP fields at a peak intensity of 1.3×10^{15} W/cm^2 (background pressure is lower than 2×10^{-10} mbar), respectively. The TOF spectrum was taken with the limited condition in the position.

Figure 2 shows the ε-dependent RIMDs for Rb^{2+}, Rb^{3+} and Rb^{4+} in the polarization xy plane, where y-axis and x-axis are defined along the major and minor polarization axis, respectively. For $\varepsilon = 0$ (the linear polarization along the y-axis), the RIMDs display two-dimensional Gaussian-like distributions with the maxima at zero position. As is expected, the distribution is expanded in the polarization direction (y-axis). For Rb^{2+}, Rb^{3+} and Rb^{4+} ions, the ratios of the RIMDs along the major axis to the minor axis are 2.2, 3.0 and 3.5, respectively. As ellipticities increase, the RIMDs split into multi-band structures along the minor axis (x-axis) of the polarization ellipse and the gap between each peaked band increases with the ellipticity, whereas the distribution along the major axis is close to Gaussian. This anisotropy is not caused by the different resolutions along the x direction and y direction of the MOTRIMS, because the peak structure reappears when the polarization ellipse is rotated by 90°. At $\varepsilon = 0.7$, two-, three- and four-band structures are presented for Rb^{2+}, Rb^{3+} and Rb^{4+}, respectively. The distributions are more likely to be clustered around the minor axis. This is due to the

fact that the amplitudes of the electric field in the y direction are stronger than those in the x direction, and thus the electrons prefer emission along the y axis. The electron that emits along the y axis at the times of y maximum of the electron field achieves a final momentum with a large x component.[21] In the case of close-to CP fields, the RIMDs of Rb^{2+}, Rb^{3+}, and Rb^{4+} show a circularly symmetric structure, two concentric rings, and a connected one part structure, respectively. Moreover, these distributions are relatively isotropic.

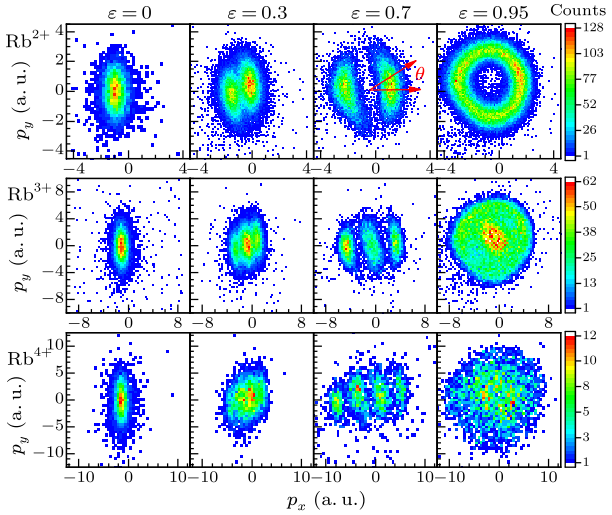

Fig. 2. Measured RIMDs in the polarization plane for different ellipticities ε (columns) from LP to close-to CP fields for double, triple, and quadruple ionizations (rows) of neutral Rb atoms. The major polarization and the minor polarization axis are along the y and x axes, respectively. The offset angle θ, indicated in the panel for $\varepsilon = 0.7$, is defined as the angle between the maximum of the RIMDs and the minor polarization axis of the laser electric field. The peak intensity of the laser pulse is about 1.3×10^{15} W/cm^2.

For Rb^{2+} at $\varepsilon = 0.7$, the two peaks are shifted by an offset angle θ marked in Fig. 2, that is, the angle between the maximum of the RIMDs and the minor axis of the polarization ellipse. Recently, much attention has been concentrated on exploring the physical mechanism of this angle shift. Previous studies have shown that the θ angle is wholly or partially caused by the long-range Coulomb interaction between the outgoing electron and the ionic core.[15] In addition, some explanations attribute the offset angle to the nonzero initial momentum at the tunnel exit in the polarization plane, and the angle shift relies heavily on the initial conditions of the electron right after the tunneling in the model, such as its momentum, position and/or a finite tunneling time.[35,36] However, all these explanations are model dependent, it is still controversial to draw a final conclusion. In Ref. [37], it was found that for Ar in the tunneling region this angle is of the order of 10°–15°, whereas the angle for He was 5°–10°. The offset angle observed in the present experiment is of the order of 45°–55°. The results show that the offset angle of the Rb atoms is significantly larger than Ar and He atoms. The interpretation of the offset angle measured in our experiment requires further theoretical investigation. This angle shift has been widely analyzed in attoclock measurements, which allows resolving photoelectron dynamics with attosecond precision with available femtosecond laser pulses.[15]

To better understand the physical mechanism of these shape characteristics, a quantitative explanation of our experimental results in terms of over-barrier ionization in close-to CP fields is presented as follows. First, we will give a brief description of the classical over-barrier ionization model. Taking an electron residing in one-dimensional potential along the field direction for instance,[38] the quasi-static electric field of increasing strength will further suppress the Coulomb barrier until the electron is no more bound when reaching the critical field strength $I_p^2/4Z$, where I_p is the ionization energy for producing an ion of a charge Z. Assuming that each electron is ionized with zero initial momentum and the ion-core Coulomb attraction can be neglected after ionization, the momentum of each electron at the end of the pulse is given by $p = I_p^2/4Z\omega$. The direction of the final momentum is perpendicular to E. At this time, the corresponding field intensity can be estimated by $I_{OBI} = I_p^4/16Z^2$. According to this explanation, the over-barrier intensity I_{OBI} of Rb^+, Rb^{2+}, $Rb^{3+}$and Rb^{4+} ions can then be estimated to be 1.8×10^{11} W/cm^2, 5.6×10^{14} W/cm^2, 1.0×10^{15} W/cm^2, and 1.9×10^{15} W/cm^2, respectively. In this case, Rb^+, Rb^{2+} and Rb^{3+} ions are generated well above the over-barrier ionization region while Rb^{4+} ions are generated around the over-barrier ionization region for the laser intensity used in our experiment. It should be noted that in the over-barrier ionization region, the RIMDs no longer depend on the laser intensity. Indeed, we have further examined the spectra of a wide range of higher laser intensities and almost identical results are obtained.

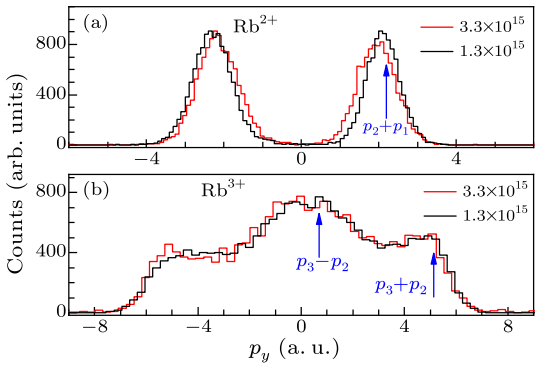

Fig. 3. RIMDs of Rb^{2+} [panel (a)] and Rb^{3+} [panel (b)] ions projected onto the y axis (along the TOF direction) for close-to CP fields at peak intensity of 1.3×10^{15} W/cm^2 (black) and 3.3×10^{15} W/cm^2 (red). The vertical arrows in (a) and (b) indicate the locations expected for the over-barrier ionization model, as discussed in the text.

To be more intuitive, Fig. 3 shows the p_y spectra (in the TOF direction where the best resolution is achieved) of Rb^{2+} and Rb^{3+} ions at peak intensities of 1.3×10^{15} and 3.3×10^{15} W/cm^2. It is clear

that the shape of the spectra is independent of laser intensities, which was expected in the over-barrier ionization region. Moreover, Rb^{2+} ions show a double-peak structure and Rb^{3+} ions show a four-peak structure. According to classical calculations for the noble gas system, the momentum spectra exhibit double-, four- and eight-peak structures for singly, doubly and triply charged ions, respectively,[21,39] due to the different combinations of the electron emitting directions. The observed momentum distribution of Rb^{2+} (Rb^{3+}) is equivalent to that of the singly (doubly) charged noble gas ions as predicted by the classical model. It happens because the first and second ionization potentials are for Rb 2.6 eV (excited state) and 27.3 eV, respectively, corresponding to over-barrier fields of 0.0023 a.u. and 0.1259 a.u., and the corresponding momentum values are about 0.04 a.u.(p_1) and 2.21 a.u.(p_2). If the two electrons were released only as the instant, the laser field would reach these two values, not only the magnitudes of p_1 and p_2 would be unique, but also the angle between them. Note that a much more likely scenario is that the electrons were released over a time range when the field is near the over-barrier value. If this time range is larger than the optical cycle, the corresponding angle range will be more than 2π. In this case one obtains recoil momenta which range between $p_2 + p_1 = 2.2492$ a.u. (when the two electrons emit into the parallel directions) and $p_2 - p_1 = 2.1690$ a.u. (when the two electrons emit into the antiparallel directions). Averaging over all possible angles between p_1 and p_2, the RIMDs will exhibit two peaks positioned at 2.25 a.u. and 2.17 a.u. However, since the difference (about 0.0802 a.u.) between $p_2 + p_1$ and $p_2 - p_1$ is even smaller than the instrumental resolution (∼0.12 a.u. for Rb^+), the expected double-peak structure is indistinguishable for the peaks around ±2.20 a.u. as shown in Fig. 3(a). From the discussion above, the following conclusions are drawn: the momentum of the first ionized electron is so small that its effects can be ignored when analyzing the ionization mechanism of higher charge states.

Next, let us move one step further for Rb^{3+}, the third ionization potential of Rb is 39.2 eV, corresponding to momentum of the third ionized electron $p_3 = 3.0365$ a.u. For the ellipticity value discussed here, the field along the x direction drives the emitted electrons transversely and effectively eliminates the possibility of recollision, so all triple ionization obtained can be regarded as originating from sequential processes. Therefore, when the second and the third electrons emit in the same direction, the total momentum value of Rb ion core $p_{\rm ion}$ is the sum of p_2 and p_3; i.e., $p_{\rm ions} = p_3 + p_2 = 5.2456$ a.u. When the two electrons emit in the opposite directions, the total momentum value of the ion core, however, is $p_{\rm ions} = p_3 - p_2 = 0.8274$ a.u. As shown in Fig. 3(b), the Rb^{3+} spectra show a four-peak structure near ±0.8 a.u. (two inner peaks) and near ±5.2 a.u. (two outer peaks). Interestingly, we find that the measured results of Rb^{2+} and Rb^{3+} ions are consistent with the classical over-barrier ionization model.

In summary, employing recently developed MOTRIMS combining with cold atoms, strong laser pulse, and ultrafast technologies, we have investigated up to quadruple ionization of neutral Rb target by EP fields. The ion momentum spectra exhibit characteristic multi-band structures as the ellipticity varies from the LP to CP fields. Theoretical analysis shows that the momentum of the first ionized electron is so small that its effects can be ignored when analyzing the physical mechanism of higher charge states, this can be verified from the RIMDs of Rb^{2+} by close-to CP fields. Accordingly, the spectra of Rb^{3+} can be interpreted quantitatively in terms of the two-successive classical over-barrier ionization model. The quantitative agreement between the classical model and our experiment results provides strong support to the classical treatment of the multielectron processes induced by strong laser fields, which is currently indispensable because the nonperturbative quantum treatments of the complex effect are not feasible.

We acknowledge the support from Shanghai-XFEL beamline project (SBP) and Shanghai High repetition rate XFEL and Extreme light facility (SHINE).

References

[1] Agostini P, Fabre F, Mainfray G, Petite G and Rahman N K 1979 *Phys. Rev. Lett.* **42** 1127
[2] Deng Y K, Li M, Yu J Z, Liu Y X, Liu Y Q and Gong Q H 2014 *Chin. Phys. Lett.* **31** 064207
[3] Wu C Y, Yang Y D, Liu Y Q, Gong Q H, Wu M, Liu X, Hao X L, Li W D, He X T and Chen J 2012 *Phys. Rev. Lett.* **109** 043001
[4] Li M, Geng J W, Liu H, Deng Y K, Wu C Y, Peng L Y, Gong Q H and Liu Y Q 2014 *Phys. Rev. Lett.* **112** 113002.1
[5] Becker W, Liu X J, Ho P J and Eberly J H 2012 *Rev. Mod. Phys.* **84** 1011
[6] Corkum P B 1993 *Phys. Rev. Lett.* **71** 1994
[7] Chen Z J, Liu F and Wen H 2019 *Chin. Phys. B* **28** 123401
[8] Yu B H, Li Y B and Tang Q B 2013 *Chin. Phys. B* **22** 013206
[9] Huang Y D, Meng C, Wang X W, Lu Z H, Zhang D W, Chen W B, Zhao J, Yuan J M and Zhao Z X 2015 *Phys. Rev. Lett.* **115** 123002
[10] Mcpherson A, Gibson G, Jara H, Johann U, Luk T S, Mcintyre I A, Boyer K and Rhodes C K 1987 *J. Opt. Soc. Am. B* **4** 595
[11] Ge P P, Han M, Deng Y K, Gong Q H and Liu Y Q 2019 *Phys. Rev. Lett.* **122** 013201
[12] Quan W, Serov V V, Wei M Z, Zhao M, Zhou Y, Wang Y L, Lai X Y, Kheifets A S and Liu X J 2019 *Phys. Rev. Lett.* **123** 223204
[13] Krausz F and Ivanov M 2009 *Rev. Mod. Phys.* **81** 163
[14] Wang X W, Wang L, Xiao F, Zhang D W, Lü Z H, Yuan J M and Zhao Z X 2020 *Chin. Phys. Lett.* **37** 023201
[15] Cirelli C, Smolarski M, Abu-Samha M, Madsen L B and Dimitrovski D 2012 *Nat. Phys.* **8** 76
[16] Zhou Y M, Huang C, Liao Q and Lu P X 2012 *Phys. Rev. Lett.* **109** 053004
[17] Huang Y, Qin C C, Zhang Y Z, Wang X C, Yan T M and Jiang Y H 2019 *Chin. Phys. B* **28** 093202
[18] Hao J X, Hao X L, Li W D, Hu S L and Chen J 2017 *Chin. Phys. Lett.* **34** 043201
[19] Tan J, Zhou Y M, He M R, Chen Y B, Ke Q H, Liang J T, Zhu X S, Li M and Lu P X 2018 *Phys. Rev. Lett.* **121** 253203
[20] Pfeiffer A N, Cirelli C, Smolarski M, Dorner R and Keller U 2011 *Nat. Phys.* **7** 428

[21] Wang X and Eberly J H 2012 *Phys. Rev. A* **86** 013421
[22] Mergel V, Jagutzki O, Spielberger L, Ullrich J and Moshammer R 2000 *Phys. Rep.* **330** 330.2
[23] Eppink A T J B and Parker D H 1997 *Rev. Sci. Instrum.* **68** 3477
[24] Wang Z M and Elliott D S 2000 *Phys. Rev. Lett.* **84** 3795
[25] Collins C B, Curry S M, Johnson B W, Mirza M Y, Chellehmalzadeh M A, Anderson J A, Popscu D and Popescu I 1976 *Phys. Rev. A* **14** 1662
[26] Li R Y, Yuan J Y, Wang X C, Hou X Y, Zhang S, Zhu Z Y, Ma Y X, Gao Q, Wang Z Y, Yan T M, Qin C C, Li S, Zhang Y Z, Weidermuller M and Jiang Y H 2019 *J. Instrum.* **14** P02022
[27] Knoop S, Morgenstern R and Hoekstra R 2004 *Phys. Rev. A* **70** 050702
[28] Knoop S, Hasan V G, Ott H, Morgenstern R and Hoekstra R 2006 *J. Phys. B: At. Mol. Opt. Phys.* **39** 2021
[29] Trachy M L, Veshapidze G, Shah M H, Jang H U and DePaola B D 2007 *Phys. Rev. Lett.* **99** 043003
[30] Blieck J, Flechard X, Cassimi A, Gilles H, Girard S and Hennecart D 2008 *Rev. Sci. Instrum.* **79** 103102
[31] Scielzo N D, Freedman S J, Fujikawa B K and Vetter P A 2004 *Phys. Rev. Lett.* **93** 102501
[32] Gorelov A, Melconian D, Alford W P, Ashery D, Ball G, Behr J A, Bricault P G, D'Auria J M, Deutsch J and Dilling J 2005 *Phys. Rev. Lett.* **94** 142501
[33] Wustelt P, Moller M, Rathje T, Sayler A M, Stohlker T and Paulus G G 2015 *Phys. Rev. A* **91** 031401
[34] Alnaser A S, Tong X M, Osipov T, Voss S, Maharjan C M, Shan B, Chang Z and Cocke C L 2004 *Phys. Rev. A* **70** 023413
[35] Camus N, Yakaboylu E, Fechner L, Klaiber M, Laux M, Mi Y, Hatsagortsyan K Z, Pfeifer T, Keitel C H and Moshammer R 2017 *Phys. Rev. Lett.* **119** 023201
[36] Landsman A S and Keller U 2015 *Phys. Rep.* **547** 1
[37] Shvetsov-Shilovski N I, Dimitrovski D and Madsen L B 2012 *Phys. Rev. A* **85** 023428
[38] Nubbemeyer T, Gorling K, Saenz A, Eichmann U and Sandner W 2008 *Phys. Rev. Lett.* **101** 233001
[39] Maharjan C M, Alnaser A S, Tong X M, Ulrich B, Ranitovic P, Ghimire S, Chang Z, Litvinyuk I V and Cocke C L 2005 *Phys. Rev. A* **72** 041403